Published in final edited form as:
Clin Cancer Res. 2010 December 1; 16(23): 5664–5678. doi:10.1158/1078-0432.CCR-10-1564.

Heterogeneous Blood-Tumor Barrier Permeability Determines Drug Efficacy in Experimental Brain Metastases of Breast Cancer

Paul R. Lockman[1,*], **Rajendar K. Mittapalli**[1], **Kunal S. Taskar**[1], **Vinay Rudraraju**[1], **Brunilde Gril**[2], **Kaci A. Bohn**[1], **Chris E. Adkins**[1], **Amanda Roberts**[1], **Helen R. Thorsheim**[1], **Julie A. Gaasch**[3], **Suyun Huang**[4], **Diane Palmieri**[2], **Patricia S. Steeg**[2], and **Quentin R. Smith**[1]

[1]Department of Pharmaceutical Sciences, Texas Tech University Health Sciences Center, Amarillo, TX.

[2]Women's Cancers Section, Laboratory of Molecular Pharmacology, Center for Cancer Research, National Cancer Institute, Bethesda, MD.

[3]Department of Life, Earth and Environmental Sciences, West Texas A&M University, Canyon, TX.

[4]Department of Neurosurgery, MD Anderson Cancer Center, Houston, TX

Abstract

Purpose—Brain metastases of breast cancer appear to be increasing in incidence, confer significant morbidity, and threaten to compromise gains made in systemic chemotherapy. The blood-tumor barrier (BTB) is compromised in many brain metastases, however, the extent to which this influences chemotherapeutic delivery and efficacy is unknown. Herein, we answer this question by measuring BTB passive integrity, chemotherapeutic drug uptake, and anticancer efficacy *in vivo* in two breast cancer models that metastasize preferentially to brain.

Experimental Design—Experimental brain metastasis drug uptake and BTB permeability were simultaneously measured using novel fluorescent and phosphorescent imaging techniques in immune compromised mice. Drug-induced apoptosis and vascular characteristics were assessed using immunofluorescent microscopy.

Results—Analysis of >2000 brain metastases from two models (human 231-BR-Her2 and murine 4T1-BR5) demonstrated partial BTB permeability compromise in >89% lesions, varying in magnitude within and between metastases. Brain metastasis uptake of ^{14}C- paclitaxel and ^{14}C-doxorubicin was generally greater than normal brain but <15% of that of other tissues or peripheral metastases, and only reached cytotoxic concentrations in a small subset (~10%) of the most permeable metastases. Neither drug significantly decreased the experimental brain metastatic ability of 231-BR-Her2 tumor cells. BTB permeability was associated with vascular remodeling and correlated with over expression of the pericyte protein, desmin.

Conclusions—This work demonstrates that the BTB remains a significant impediment to standard chemotherapeutic delivery and efficacy in experimental brain metastases of breast cancer.

Reprint Requests: Paul Lockman, Texas Tech University Health Sciences Center, 1406 Coulter, Amarillo, TX 79106. Phone: 806.356.4750 x 227, (Paul.Lockman@ttuhsc.edu)..

Author Contributions R.K.M., K.S.T., V.R., B.G., K.A.B., C.E.A., F.C.T., H.R.T., J.A.G. performed experimental studies. S.H. developed the 4T1-BR5 cell model. R.K.M., K.S.T., V.R. and K.A.B. contributed equally to this paper. P.R.L., D.P., P.S.S., and Q.R.S. designed and analyzed experiments, and wrote the manuscript. All authors discussed the results and commented on the manuscript.

New brain permeable drugs will be needed. Evidence is presented for vascular remodeling in BTB permeability alterations.

Keywords

Brain metastases; breast cancer; blood-tumor barrier; paclitaxel; doxorubicin

Introduction

Historically, brain metastases occurred in 10-20% of patients with disseminated breast cancer after the development of systemic lung, liver and bone metastases. In such patients, treatment has been primarily palliative with brain metastases rarely being the cause of death (1,2). In recent years, however, the rate of brain metastasis has increased, approaching or exceeding 35% in subpopulations of metastatic breast cancer patients, particularly those with Her2+ or “triple-negative” (estrogen and progesterone receptor negative, Her2 normal) tumors (3-5). The causes for this increase may be multiple, including improved systemic therapy, more frequent imaging, and the “sanctuary site” status of the brain. The net effect is that the patient experience is changing (6), with brain metastases more commonly presenting in patients who are responding to systemic therapy or have stable disease, and patients are succumbing to brain metastases (7). Clearly, a porportion of breast cancer patients are doing well systemically when brain metastases occur, and need effective treatments for CNS disease.

Current therapy for brain metastases of breast cancer involves radiation and surgery (1,2). Stereotactic radiosurgery delivers a large dose of radiation to a defined brain lesion, while whole brain radiotherapy irradiates the entire brain to treat multiple metastases and prevent the outgrowth of occult micrometastases. Surgery can remove one-to-several lesions in favorable locations. Steroids are used to control edema. The role of chemotherapy has been limited (8) as clinical trials of standard breast cancer drugs have provided disappointing results (9-11). Similar findings occur with other cancer histologies that metastasize to brain (12). Multiple strategies have been explored with limited success to improve brain tumor chemotherapy, including combination with radiation, novel formulations, direct administration into the central nervous system, and targeted vascular disruption (8,13). Both disease progression and treatments cause significant patient morbidity, including cognitive defects.

One of the reasons listed for the failure of brain chemotherapy is presence of the blood-brain barrier (BBB), which is located at the brain vascular endothelium (14). The BBB has low passive paracellular permeability and expresses high levels of active efflux drug transporters, which together limit brain exposure for many anticancer agents (15,16). Included in this are two of the most widely used breast cancer chemotherapeutics – paclitaxel and doxorubicin, which are excluded from brain by BBB P-glycoprotein efflux transport (17-20).

The BBB is frequently impaired in brain metastases, creating the blood-tumor barrier (BTB) (21). The extent to which this compromise impacts CNS chemotherapy has been controversial for over 30 years (14,22-28). Many, but not all, brain metastases display elevated BTB permeability, as demonstrated by MRI contrast enhancement to electron-dense tracers (1,21). However, quantitative information is sparse on the relationship between BTB breakdown and chemotherapeutic drug delivery and activity in brain metastases. Few measurements have been made of chemotherapeutic drug exposure to brain metastases in humans or experimental animals (15,29-31). The database is somewhat better for primary brain tumors (26,29,30,32-38), but most drug penetration data are from studies of normal

brain. Animal studies of drug distribution in brain metastases have been limited by non-physiologic tumor models involving direct intracerebral tumor cell injection and by analytic methods that fail to capture the full heterogeneity of drug distribution within brain tumors. Further, no studies have correlated drug levels in brain metastases with BTB passive permeability, transporter expression, and direct tumor cytotoxic effect.

Herein, we explore these questions using two recently established experimental models of brain metastasis that arise from the systemic circulation (39,40). One involves the brain-colonizing subline (231-BR) of the metastatic triple-negative MDA-MB-231 human breast cancer cell line, which was isolated by repeated cycles of intra-cardiac injection and harvesting from brain metastases (40,41). This model, when compared to human brain metastases of breast cancer, was found to have equivalent rates of proliferation and apoptosis (42), and a prominent neuro-inflammatory response (42). Further, 231-BR brain metastases are contrast-enhancing by MRI (43), supporting the relevance of this model to human disease. In this study we have used a Her2 transfectant of 231-BR expressing enhanced green fluorescent protein (eGFP). This transfectant was chosen because it produced greater numbers of brain metastases than the parent cell line (40). The second model was derived using the murine 4T1 mammary breast cancer cell line (44). Novel quantitative fluorescent and phosphorescent imaging techniques were used with these models to assess the patency of the BTB to passive permeability markers and the degree of uptake of radiolabeled chemotherapeutic drugs. Results were then correlated, in the same lesions, with cleaved caspase-3 staining as a molecular marker of drug-induced apoptosis. Further drug efficacy was tested in a 4-week experimental brain metastasis assay. This integrated approach allowed us to address three important questions: a) to what extent does brain metastasis drug distribution correlate with BTB-induced changes in integrity? b) What level of brain metastasis drug exposure is associated with chemotherapeutic effect? and c) Do changes in BTB integrity between metastases correlate with BTB architecture, such as histological structure, vascular density (angiogenesis) or pericyte expression?

Materials and Methods

Experimental metastasis assays

Female NuNu mice were anesthetized with isofluorane and inoculated with one of two breast cancer cell lines (231-BR-Her2: 1.75×10^5. 4T1-BR5: 5×10^4) in the left cardiac ventricle (Supplementary Fig. 1). Tumors seeded the brain and developed over 2–6 weeks until neurological symptoms appeared.

Tracer or drug administration

Animals were anesthetized with ketamine/xylazine and administered Texas Red dextran (3 or 70 kDa, Invitrogen; 1.5 mg/animal) and/or ^{14}C-AIB (25 μC_i/animal; American Radiolabeled Chemicals), ^{14}C-paclitaxel (25 μC_i/animal, 10 mg/kg in Taxol formulation, Moravek), ^{14}C-doxorubicin (12.5 μC_i/animal, 6 mg/kg, GE Healthcare), or ^{14}C-dextran (70 kDa, 5 μC_i/animal, Moravek) into the femoral vein (Supplementary Fig. 1). Tracers circulated for 2 to 480 min, during which time blood samples ($n \leq 5$) were periodically collected to map the time course of blood exposure (45, 46). In some experiments, indocyanine green (1.5 mg/animal, Sigma) was injected *i.v.* 1 min prior to death as a near-infrared marker of vascular density (47, 48). At the end of the circulation period, animals were euthanized and brain was removed from the skull (<30 s) and flash frozen in isopentane (−65°C). In most experiments, residual intravascular tracer was washed out of brain by cardiac perfusion (5-10 mL/min) for 30-60 s immediately following death. Perfusion fluid consisted of physiologic saline (pH 7.4, 37 °C) (33) containing 6% dextran (blank) or 2.7% albumin plus 0.6 mg/mL indocyanine green to mark blood vessels. The

efficacy of the vascular washout procedure was verified as >90% in separate experiments (Supplementary Fig. 2). Samples were also collected from other tissues, as well as blood and serum, for comparative analysis. Frozen sections were cut at 20 μm with a cryostat (−23 °C) and mounted on glass slides.

Drug efficacy studies were performed with mice treated intravenously with clinical grade paclitaxel (6 mg/kg) or doxorubicin (5 mg/kg) once a week for 4 weeks and the number of metastatic lesion tabulated as previously described (49,50).

Fluorescent analysis of BTB permeability, tumor distribution, and vascular density

Fluorescence analyses were performed using an Olympus MVX10 microscope with a 2X objective (NA, 0.5) and an optical zoom of 0.63-6.3x. Excitation and emission filters were 470 ± 40 nm and 525 ± 50 nm for eGFP, 560 ± 55 nm and 645 ± 75 nm for Texas Red dextran, and 740 ± 35 nm and 780 longpass filter for near-infrared indocyanine green. Exposure time varied from 300-500 ms for initial scans of whole tissue sections to 15 ms for quantitative analysis of tumor regions. For Texas Red dextran, total fluorescence intensity in a region of interest was converted to sum voxel intensity/g tissue. Volume was calculated as area (cm^2) × 0.002 cm thickness corrected for density 1.04 g/cm^3. To convert fluorescence intensity to concentration, standard curves were generated (Supplementary Fig. 3), similar to autoradiography (46). Brain (500 mg) was excised and homogenized to uniformity with 100 μL of saline containing different concentrations of Texas Red dextran. The final mixture was flash frozen in isopentane and sliced into 20 μm sections. Similarly, blood samples were spiked with concentrations of dye, 1 μL samples were placed on glass slides and dried, and then total fluorescence intensity for the blood drop was measured. Texas Red dextran fluorescence intensity did not differ between standards prepared from brain or tumor, or from solutions of differing pH (6.0 −7.6) or Na^+/Ca^{2+} concentration (data not shown). Texas Red dextran sum intensity was stable within ± 5% with repeat fluorescent exposures (15 ms – 1500 ms). Fluorescent image analysis was performed using Slidebook 5.0 program (Olympus). Vascular density and surface area were calculated using binary masks where vessels were defined by indocyanine green fluorescence ≥3 fold above background.

Radioactive analysis and phosphorescence imaging

^{14}C Radioactivity (dpm) in tissues and fluids was determined by liquid scintillation counting, corrected for quench and background. Radiotracer imaging was performed by exposure of tissue sections to phosphor screens in cassettes for 2-14 days, followed by data analysis using a Fuji phosphoimager with tissue-calibrated ^{14}C-standards (GE Healthcare). Phosphor images were converted to color-coded ^{14}C tissue concentrations using MCID software (Imaging Research). Typical brain ^{14}C concentrations were 40-80 nCi/g for ^{14}C-AIB and 0.5-3 nCi/g for ^{14}C-paclitaxel and ^{14}C-doxorubicin. Limits of detection and quantitation equaled 0.1 and 0.3 nCi/g, respectively, for ^{14}C (Supplementary Fig. 3). *In vivo* radiotracer integrity (>80-95%) were confirmed for ^{14}C-paclitaxel and ^{14}C-doxorubicin using HPLC, as previously described (51, 52).

Kinetic analysis

Vascular passive permeability (PS) was determined by measuring the unidirectional blood-to-brain transfer coefficient (K_{in}). Briefly K_{in} was determined for ^{14}C-AIB and TX Red 3kDa uptake into normal brain in control animals using the multiple-time uptake approach (circulation time = 5-30 min) (45). BBB K_{in} was found to equal $2.9 \pm 1.1 \times 10^{-5}$ mL/s/g and $1.1 \pm 0.4 \times 10^{-5}$ mL/s/g, respectively (n=8-10). BBB K_{in} was converted to vascular permeability-surface area product (PS) using the equation

$$PS = -F \ln (1 - K_{in}/F) \quad (1)$$

where F = cerebral blood or serum flow (45,53). In this paper, BTB K_{in} was taken as equivalent to PS as, even with the highest BTB K_{in} values in brain metastases (i.e., 35 fold elevation for ^{14}C-AIB), K_{in} differed from PS by less than 10%. Cerebral blood flow was measured using ^{14}C-nicotine (54) and was reduced 30-70% in most brain metastases (data not shown). Once normal BBB PS was established for control animals, single-time uptake (10 min) was used to measure PS in most animals (46). Individual metastasis PS and drug concentrations were considered elevated when they exceeded mean + 3 S.D. of matching normal brain.

Cresyl Violet Staining

Sections were fixed in 4% paraformaldehyde in PBS for 10 min, rinsed and immersed in 0.1% cresyl violet acetate (15 min) and rinsed again. Sections were processed for differentiation, dehydration, and clearing in 70% ethanol (15 s), 95% ethanol (30 s), 100% ethanol (30 s), respectively. Brightfield images were captured with a 2x objective and superimposed on fluorescent images to co-localize drug or tracer permeability.

Immunofluorescence

Tissues were rehydrated in PBS and then fixed in either cold acetone for collagen type IV (Millipore) and desmin antibody (Dako), ice-cold methanol for ABCB1 (Santa Cruz Biotechnology), or cold 4% PFA for cleaved caspase-3 (Cell Signaling), and cytokeratin (Abcam). After 3 PBS washings (5 min), they were blocked with either 4% or 10% goat serum, or 0.2% Triton-X 100 (1h). Primary antibodies were added, followed by overnight incubation at 4°C. CD31 antibody (BD Pharmingen) was co-incubated with each of the previous antibodies. After washing, secondary antibodies and/or DAPI (1 mg/mL) were added (1 h). Slides were washed, DAKO mounting medium was added, and coverslips were applied. For each metastasis within a section identified as permeable or non-permeable, CD31+ blood vessels were manually identified and the surface area (μm^2) of the vessel calculated along with the signal intensity of desmin, collagen type IV or ABCB1 per vessel. For each metastasis, the results are shown as a ratio of the mean antibody intensity per total vessel area.

Statistical Analysis

Prism 5 software was used to analyze the data. Results are presented as mean ± S.D. Statistical differences were assessed using nonparametric Mann Whitney or Kruskal Wallis tests. Pearson's correlation was used to calculate r^2. All tests were two-sided with $p<0.05$ for statistical significance. The D'Agostino-Pearson omnibus K2 normality test was used to determine if data conformed to the normal distribution. Statistical p values obtained with this test for normal brain were p=0.232 for ^{14}C-paclitaxel (n=257), p=0.220 for ^{14}C-doxorubicin (n=118), and p=0.143 for AIB PS (n=133).

Results

BTB permeability

BTB integrity was assessed from measured passive permeability (PS) changes using two markers, 103 Dalton ^{14}C- AIB and 3kDa Texas Red dextran, which bracket the molecular weight range of most non-biologic chemotherapeutic drugs (Fig. 1). For both models, metastatic lesions were operationally defined as cancer cell clusters within 100 μm of each other, based on the diffusion limit of oxygen. Using this definition, metastases ranging in

size from ~300 μm to ~3 mm in diameter were observed with both the 231-BR-Her2 (Fig. 1A) and 4T1-BR5 models (Fig. 1D). Representative examples of brain sections containing multiple metastases with heterogeneous permeability are illustrated in Fig. 1B-C, and Fig. 1E-F. The cumulative data for n=686 231-BR-Her2 and n=892 4T1-BR5 brain metastases show that a) >89% of brain metastases exhibited statistically increased BTB permeability compared to normal brain to one or both markers, b) changes in permeability were intermediate (1.5-3.2 fold) in most cases (37-76% of metastases), and c) in only a subset (0.8-26% of metastases) were there prominent permeability changes, defined as >10 fold for AIB and >5 fold for Texas Red 3kDa dextran (Fig. 1G-H). Changes in permeability were noted for both markers across the range of metastases from small micrometastases (<1 mm diameter) to large, clinically detectable lesions (>1 mm diameter). A significant correlation of permeability ($r^2 = 0.54$) was observed for the two permeability markers when measured in the same lesions (Fig. 1I). However, no clear relationship was observed between permeability and lesion size (r^2 ranged from 0.09 to 0.23 for both markers in both models) (Fig. 1J-L) or morphology (e.g., compact vs. diffuse) (Supplementary Fig. 4-5). Comparable results were found in metastases without vascular washout (Supplementary Fig. 6). The results show that most brain metastases exhibit increased BTB passive permeability compared to normal brain with marked heterogeneity both in small and larger metastases.

Brain metastasis distribution of paclitaxel

Next, we asked the question whether and to what extent variable BTB permeability alterations translated into differential uptake of two commonly used breast cancer chemotherapeutic agents, paclitaxel and doxorubicin at pharmacologic doses. Representative images for 231-BR-Her2 metastases are shown in Fig. 2A-F. Paralleling what was found in BTB passive permeability, ^{14}C-paclitaxel concentrations were heterogeneous both between (Fig. 2A-C) and within (Fig. 2D-F) metastases, with some lesions increasing by >200 fold. In a cumulative analysis involving n=379 231-BR-Her2 brain metastases, ^{14}C-paclitaxel concentrations were elevated in 85% of lesions, with the majority (47%) increasing by <10 fold and only a small subset (10%) increasing by >50 fold (Fig. 2G). Average brain metastasis ^{14}C-paclitaxel concentration significantly exceeded normal brain by 10-20 fold at all time points from 30 min to 8 hrs ($p<0.05$) (Fig. 2H), but was at least an order of magnitude less than that of peripheral tissues, such as liver or kidney ($p<0.05$). Radiochemical integrity was confirmed as >95% in serum and brain by HPLC at 30 min and 2 hr and >80% at 8 hr. No clear correlation was found between metastasis ^{14}C-paclitaxel concentration and lesion size (Fig. 2I) or morphology (Supplementary Fig. 7), whereas an appreciable correlation ($r^2 = 0.59$) was noted with BTB passive permeability to 3kDa Texas Red (Fig. 2J). Similar trends were observed for ^{14}C-paclitaxel distribution in 4T1-BR5 brain metastases (Fig. 3A-E). In a number of 4T1-BR5 injected animals, metastases were found in peripheral tissues (e.g., liver, kidney, lung) with ^{14}C-paclitaxel concentrations (6000–30,000 ng/g; Fig. 3F-H), notably higher than brain metastases in the same animals (150 – 2000 ng/g). The data are consistent with the hypothesis that BTB function, though partially compromised, is still present and limits drug delivery to a significant extent relative to that found in non-CNS metastases or peripheral tissues.

Paclitaxel rarely induced apoptosis in brain metastatic tumor cells and did not show significant efficacy

To determine if paclitaxel achieved cytotoxic concentrations in brain metastases, 231-BR-Her2 brain sections from animals exposed to paclitaxel for 8 hr were stained for cleaved caspase-3 as a marker of apoptosis (55,56). As shown in a representative experiment (Fig 4A-C), multiple tumor cells exhibiting enhanced cleaved caspase-3 staining were found in brain metastases with ^{14}C-paclitaxel concentrations >1000 ng/g, whereas little or no staining was found in low ^{14}C-paclitaxel 231-BR-Her2 metastases (<200 ng/g) (Fig. 4D-F). Similar

data were also observed in the 4T1-BR5 brain metastasis model (Supplementary Fig. 8). The results demonstrate that paclitaxel-induced cytotoxic effects occur only in a small subset (~10%) of brain metastasis regions that have markedly elevated paclitaxel concentrations (>1000 ng/g).

The ability of paclitaxel to reduce the number and size of 231-BR-Her2 metastatic lesions in the brain was tested. Weekly treatment of 6 mg/kg paclitaxel was administered 3 days post-injection of tumor cells for 4 weeks. At necropsy, brains were dissected saggittally and ten sections, one every 300 microns, from one hemisphere were H&E stained. The number of micro- and large metastases were tabulated as previously described (49,50). Paclitaxel-treated mice had a mean of 175 (95% confidence interval: 103-247) micrometastases and 6.9 (2.9-10.8) large metastases per section compared to vehicle control-treated mice with 128 (99-175) and 6.9 (4.9-9), respectively. Thus, the low degree of apoptosis observed agreed with ineffective chemotherapeutic ability, despite the fact that the 231-BR-Her2 cell line is sensitive to paclitaxel *in vitro* with an IC_{50} of 4-6 nM (data not shown).

Brain metastasis distribution of doxorubicin

To determine if other chemotherapeutic drugs behaved similarly to paclitaxel, matching experiments were conducted with ^{14}C-doxorubicin (6 mg/kg, *i.v.*, 30 min) in the 231-BR-Her2 (Fig. 5A-C) and 4T1-BR5 (Fig. 5D-F) models. ^{14}C-Doxorubicin uptake varied widely among brain metastases in both models, and like paclitaxel, correlated significantly with BTB passive permeability increases to Texas Red 3kDa dextran (Fig. 5H). The range of observed ^{14}C-doxorubicin concentrations varied from 30 to >1300 ng/g among brain metastases (Fig. 5G-I), with similar findings for both drugs in animals that were not subjected to vascular washout (Supplementary Fig. 9). ^{14}C-Doxorubicin integrity was confirmed by HPLC as >95%. Similar to paclitaxel, doxorubicin also was not efficacious in inhibiting the number or size of 231-BR-Her2 metastatic lesions in the brain. Doxorubicin administered at a 5 mg/kg dose once a week for 4 weeks yielded a mean of 144 (109-179) micrometastases and 5.2 (3.4-7) large metastases per section compared to vehicle control treated mice with 128 (99-175) and 6.9 (4.9-9), respectively. The results support the conclusion that variable drug distribution is generalizable across both models. Most experimental brain metastases attained low drug concentrations (<200 ng/g) which were not efficacious *in vivo*.

Correlation between BTB permeability and vascular remodeling

The causes of BTB heterogeneity within metastases of the same brain are unknown. The role of angiogenesis in brain metastasis formation is debated, with several reports showing co-option of existing vasculature by intravasated tumor cells (57,58), while other reports support a role of vascular endothelial growth factor-induced angiogenesis (59). Therefore, we tested whether vascular density, as a standard measure of angiogenesis, was greater in BTB permeable vs nonpermeable metastases. Representative brain sections from animals injected with indocyanine green as a vascular marker are shown in Fig. 6A-C. The combination of Texas Red 3kDa dextran and indocyanine green allowed simultaneous quantitative imaging of BTB PS and vascularity, respectively, in individual metastases, as shown in representative images for one permeable (Fig. 6G-J) and nonpermeable lesion (Fig. 6K-N). No increase was observed in vascular density for permeable lesions in either model (Fig. 6D). Further, no increase was noted when groups were plotted vs. metastasis size (Fig. 6E-F).

If the extent of angiogenesis does not explain the variable BTB integrity of experimental brain metastases, vascular remodeling or normalization could be contributory (60). Therefore, expression levels were determined by staining for three BTB components;

pericyte desmin protein, basement membrane collagen type IV, and endothelial ABCB1 P-glycoprotein efflux transporter in permeable and nonpermeable 231-BR-Her2 brain metastases. Briefly, brain sections were evaluated for 3kDa Texas Red dextran immunoflourescence to identify permeable and nonpermeable metastases. On the adjacent brain section, the relative expression level of each BTB component was determined by co-immunoflourescence in every visible capillary within a metastasis, and normalized to CD31 capillary area using an automated imaging system. When the mean expression levels of 15 permeable and 20 nonpermeable metastases were compared, an association was observed for high desmin expression in permeable metastases ($p=0.0005$) (Fig. 7A-B). When similar staining was performed for basement membrane collagen type IV, a trend toward lower collagen expression was observed in permeable lesions (Fig. 7C-D). This pattern is opposite that for desmin, and is consistent with specific BTB remodeling. No clear relationship was observed between ABCB1 P-glycoprotein efflux transporter expression level and metastasis passive permeability (Fig. 7E). The association of enhanced pericyte desmin protein with elevated permeability may suggest a role of vascular remodeling in BTB compromise.

Discussion

This study, through a combination of sensitive fluorescence and phosphorescence imaging methods, provides quantitative insights into the relationships between BTB integrity, drug delivery, and drug action in two models of brain metastases of breast cancer. The results show clearly for the first time that, while the BTB is impaired in most brain metastases, residual BTB function generally limits paclitaxel and doxorubicin distribution to subtherapeutic levels. For paclitaxel, cytotoxic concentrations (i.e., cleaved caspase-3 staining) were reached only in a subset (<10%) of the leakiest brain metastases where drug concentration exceeds 1000 ng/g. In opposition, drug concentrations in systemic metastases (outside the CNS) exceeded those in brain lesions by >10 fold, and many tissues outside the brain had drug concentrations ranging from 10,000-100,000 ng/g. In agreement with these data, treatment with paclitaxel or doxorubicin did not reduce metastatic burden in the brain when the drugs were administered over a 4 week time course of assay. The results highlight the impact of the BBB and BTB to compromise therapeutic efficacy of poorly penetrating chemotherapeutic agents in brain metastases of breast cancer.

This study also provides valuable new methodology for combined quantitative analysis of barrier integrity and drug distribution in experimental animal models. While fluorescent indicators of BBB integrity have been reported previously, these methods have generally been qualitative and have not allowed analysis of marker distribution in small regions (<1 mm^3) of brain tissue. Herein, we provide a coupled quantitative fluorescent and autoradiographic method that has been adapted from prior elegant double or triple autoradiographic techniques (61,62). This current methodology allows the quantitative measurement of changes in passive permeability and vascularity using two or more fluorescent probes and can provide data within a few hours with <1 μm resolution, as compared to days-weeks with 10-25 μm resolution using traditional autoradiography (63). Further, with ^{14}C phosphorescence, drug distribution can be mapped in 10 μm pixels at levels (~0.3 nCi/g) significantly below most other methods, including standard film autoradiography (~10 nCi/g). For example within this study brain paclitaxel measurements at the limit of quantitation for ^{14}C corresponds to concentrations of ~5 ng/g tissue, which in a small metastasis (i.e., 100 × 100 × 20 μm) represents ≤1 femtogram of drug. Overall, the method allows us the ability to dissect the roles of BTB integrity, vascular drug delivery and chemotherapeutic action in the same tissue slice.

A striking finding of this report is the marked heterogeneity of BTB integrity and drug distribution among metastases. Based upon analysis of n>2000 metastases, statistically

significant changes in BTB permeability were observed in ~90% of 231-BR-Her2 and ~96% of 4T1-BR5 brain metastases. This is consistent with the 231-BR model showing Gd-DPTA enhancement by MRI *in vivo* (43) and with limited prior observations of BTB integrity in experimental models of brain metastases of breast cancer (64,65). The data herein, show that the BTB is variably compromised in most brain metastases greater than a minimal size (>0.1-0.2 mm^2), where historically, significant integrity changes were primarily associated with large lesions (>1 - 4 mm diameter) where diffusion distances compromise oxygen and nutrient delivery and lead to angiogenesis (66). With tumor cell delivery via the vasculature, two patterns of tumor growth, compact/solid and diffuse/infiltrative, have been noted for brain metastases (64,65). Diffuse/infiltrative lesions may arise in part through perivascular tumor spread via blood vessel co-option (67,68). In our data, no clear relation was found between changes in the integrity of the BTB and metastasis size or diffuse vs. compact structure. A number of small or diffuse lesions were found with marked BTB compromise (>10 fold increase for AIB), whereas some large, compact tumors were observed with only limited elevations. The cause of this heterogeneity warrants further study.

While the BTB had observable permeability changes in most brain metastases, this should not be taken as evidence of the absence of barrier function. For brain metastases from both models, the average permeability of ^{14}C-AIB (~3 fold greater than normal brain) was <2-5% of that of peripheral breast tumor (69) or circumventricular regions of the brain without a BBB (70). Even in the leakiest of brain metastases (~33 fold increase), permeability was still <12% of that in a peripheral breast tumor (70). Similarly, average paclitaxel concentration in brain metastases was on average only 3% of levels in metastases in other tissues; even in the highest cases concentrations did not exceed 15% of that in peripheral metastases (Fig. 3F). Thus, BTB function in these models may be viewed as only partly compromised, retaining a significant ability to impede chemotherapeutic uptake.

The data also provide clear correlations between drug concentration and chemotherapeutic effect. Paclitaxel-induced apoptosis was noted only in brain metastases where drug concentrations exceeded 1000 ng/g (>1.2 μM) for both the 231-BR-Her2 and 4T1-BR5 models. Correction of this value for reported paclitaxel tissue binding [free fraction = 0.0028; (71)] suggests that apoptosis was noted only at free paclitaxel concentrations of 1.2 μM × 0.0028 = >3.4 nM. This value agrees well with the *in vitro* paclitaxel IC_{50} of 3 nM for the 231 parent cell line (72) and ~4-6 nM with the 231-BR-Her2 model. In contrast, doxorubicin, which attains similar maximum concentrations in brain metastases but is >20 times less potent (IC_{50} > 100 nM) (73) (data not shown), may not produce significant cytotoxicty in brain metastases *in vivo*. Consistent with this finding, we have not detected elevated cleaved caspase-3 staining in brain metastases from animals treated with doxorubicin. Average paclitaxel concentrations of 2507 and 1614 ng/g were reported by Fine et al. (29) in the center and periphery of human brain metastases removed by surgery. Since these values are in the same range as reported in this study, our data are consistent with limited efficacy of paclitaxel against human brain metastases (10,12).

The combined imaging methods used in this paper highlight the potential role of vascular remodeling in BTB compromise. An unexpected relationship was observed between increased desmin staining, a pericyte protein, and elevated BTB permeability. Other aspects of BTB architecture, including staining for basement membrane type IV collagen and efflux pump ABCB1, did not exhibit this trend. Most studies have observed a positive relationship between pericyte coverage and maintenance of BBB integrity and function, including upregulation of P-gp expression (rev. in (74)). However, several reports are consistent with our observations. For example, pericyte abundance or remodeling has been associated with increased BBB permeability in *in vitro* models of hypoxia and sepsis (75,76), and *in vitro* co-cultures of brain vascular cells (77,78). In one study, pericytes collaborated with

astrocytes to maintain BBB integrity under low levels of hypoxia but, during acute hypoxia, pericytes exacerbated BBB disruption (75). In another situation, the inflammatory mediator, LPS, disrupted BBB integrity *in vivo* and was associated with pericyte detachment from the basement membrane of the BBB (76). Confirmation of this trend will be attempted via electron micrographic or other non-immunological methods to ensure that increased pericyte density, rather than their accessibility to antibodies, is observed. These data provide insight into a potentially new therapeutic target to improve brain metastasis drug delivery.

Brain metastases represent an important clinical problem. In breast cancer, brain metastases are occurring when patients are either responding to systemic therapies or have stable disease, and threaten to limit the gains made in improved systemic chemo- and molecular therapies. It is probable that, as systemic chemotherapy improves for other types of cancers, brain metastases will become even more widespread. Our results support a role of the BTB in hindering chemotherapeutic treatment of brain metastases for agents that poorly penetrate the BBB, such as paclitaxel and doxorubicin. Further work is necessary to determine brain metastasis distribution of permeable chemotherapeutic agents. Given the failure of many poorly BBB-penetrable chemotherapeutic drugs, a new class of agents may be necessary for good chemotherapeutic activity against brain metastases. Such agents will not only need to be BBB permeable and active against metastatic breast cancer cells, but also non-toxic to CNS constituents. Examples in the preclinical literature to date include lapatinib and vorinostat (49,50). The concept of site-specific metastasis therapy represents a paradigm shift from a “one drug treats all sites” approach.

STATEMENT OF TRANSLATIONAL RELEVANCE

Brain metastases are prevalent in lung and breast cancers and melanoma. In metastatic breast cancer, the incidence of brain metastases approaches 35% of Her2+ or triple negative patients. Brain metastases are considered a “sanctuary site”, yet comprehensive quantitative data on blood-tumor barrier (BTB) permeability to drugs are lacking. Here, we use two models of brain metastases of breast cancer to demonstrate that (1) most metastases exhibit some increased BTB permeability; (2) permeability is poorly correlated with lesion size; and (3) only ~10% of lesions with the highest permeability exhibited cytotoxic responses to paclitaxel or doxorubicin. The data indicate that the BTB remains sufficiently intact in most experimental brain metastases to significantly impair drug delivery, and reinforces the need for brain-permeable molecular therapeutics. Finally, we report that permeable brain metastases exhibit distinct BTB remodeling, in particular, an overexpression of the pericyte protein desmin, suggesting a first molecular target to modify permeability.

Supplementary Material

Refer to Web version on PubMed Central for supplementary material.

Acknowledgments

Grant Support: Intramural Program of the National Cancer Institute (PSS, DP), grant W81XWH-062-0033 from the Department of Defense Breast Cancer Research Program (PSS, QRS, PRL, SH), and grant R01 NS052484 from NINDS/NIH (QRS).

References

1. Lin N, Bellon J, Winer E. CNS metastases in breast cancer. J Clin Oncol 2004;22:3608–17. [PubMed: 15337811]

2. Weil R, Palmieri D, Bronder J, Stark A, Steeg P. Breast cancer metastasis to the central nervous system. Am J Pathol 2005;167:913–20. [PubMed: 16192626]
3. Lin NU, Winer EP. Brain metastases: the HER2 paradigm. Clin Cancer Res 2007;13:1648–55. [PubMed: 17363517]
4. Pestalozzi BC, Zahrieh D, Price KN, Holmberg SB, Lindtner J, Collins J, et al. Identifying breast cancer patients at risk for Central Nervous System (CNS) metastases in trials of the International Breast Cancer Study Group (IBCSG). Ann Oncol 2006;17:935–44. [PubMed: 16603601]
5. Shmueli E, Wigler N, Inbar M. Central nervous system progression among patients with metastatic breast cancer responding to trastuzumab treatment. Eur J Cancer 2004;40:379–82. [PubMed: 14746856]
6. Mayer M. A patient perspective on brain metastases in breast cancer. Clin Cancer Res 2007;13:1623–4. [PubMed: 17363511]
7. Bendell J, Domchek S, Burstein H, Harris L, Younger J, Kuter I, et al. Central nervous system metastases in women who receive trastuzumab-based therapy for metastatic breast carcinoma. Cancer 2003;97:2972–7. [PubMed: 12784331]
8. Peereboom DM. Chemotherapy in brain metastases. Neurosurgery 2005;57:S54–65. discusssion S1-4. [PubMed: 16237290]
9. Boogerd W, Dalesio O, Bais EM, van der Sande JJ. Response of brain metastases from breast cancer to systemic chemotherapy. Cancer 1992;69:972–80. [PubMed: 1735089]
10. Freilich RJ, Seidman AD, DeAngelis LM. Central nervous system progression of metastatic breast cancer in patients treated with paclitaxel. Cancer 1995;76:232–6. [PubMed: 8625097]
11. Rosner D, Nemoto T, Lane WW. Chemotherapy induces regression of brain metastases in breast carcinoma. Cancer 1986;58:832–9. [PubMed: 3755076]
12. Walbert T, Gilbert MR. The role of chemotherapy in the treatment of patients with brain metastases from solid tumors. Int J Clin Oncol 2009;14:299–306. [PubMed: 19705239]
13. Gabathuler R. Blood-brain barrier transport of drugs for the treatment of brain diseases. CNS Neurol Disord Drug Targets 2009;8:195–204. [PubMed: 19601817]
14. Deeken JF, Loscher W. The blood-brain barrier and cancer: transporters, treatment, and Trojan horses. Clin Cancer Res 2007;13:1663–74. [PubMed: 17363519]
15. Motl S, Zhuang Y, Waters CM, Stewart CF. Pharmacokinetic considerations in the treatment of CNS tumours. Clin Pharmacokinet 2006;45:871–903. [PubMed: 16928151]
16. Ohtsuki S, Terasaki T. Contribution of carrier-mediated transport systems to the blood-brain barrier as a supporting and protecting interface for the brain; importance for CNS drug discovery and development. Pharm Res 2007;24:1745–58. [PubMed: 17619998]
17. Colombo T, Zucchetti M, D'Incalci M. Cyclosporin A markedly changes the distribution of doxorubicin in mice and rats. J Pharmacol Exp Ther 1994;269:22–7. [PubMed: 8169829]
18. Kemper EM, van Zandbergen AE, Cleypool C, Mos HA, Boogerd W, Beijnen JH, et al. Increased penetration of paclitaxel into the brain by inhibition of P-Glycoprotein. Clin Cancer Res 2003;9:2849–55. [PubMed: 12855665]
19. Sparreboom A, van Tellingen O, Nooijen WJ, Beijnen JH. Tissue distribution, metabolism and excretion of paclitaxel in mice. Anticancer Drugs 1996;7:78–86. [PubMed: 8742102]
20. van Asperen J, Mayer U, van Tellingen O, Beijnen JH. The functional role of P-glycoprotein in the blood-brain barrier. J Pharm Sci 1997;86:881–4. [PubMed: 9269863]
21. Gerstner E, Fine R. Increased permeability of the blood-brain barrier to chemotherapy in metastatic brain tumors: Establishing a treatment paradigm. J Clin Oncol 2007;25:2306–12. [PubMed: 17538177]
22. de Vries NA, Beijnen JH, Boogerd W, van Tellingen O. Blood-brain barrier and chemotherapeutic treatment of brain tumors. Expert Rev Neurother 2006;6:1199–209. [PubMed: 16893347]
23. Donelli MG, Zucchetti M, D'Incalci M. Do anticancer agents reach the tumor target in the human brain? Cancer Chemother Pharmacol 1992;30:251–60. [PubMed: 1643692]
24. Mellett LB. Physicochemical considerations and pharmacokinetic behavior in delivery of drugs to the central nervous system. Cancer Treat Rep 1977;61:527–31. [PubMed: 884690]

25. Muldoon LL, Soussain C, Jahnke K, Johanson C, Siegal T, Smith QR, et al. Chemotherapy delivery issues in central nervous system malignancy: a reality check. J Clin Oncol 2007;25:2295–305. [PubMed: 17538176]
26. Stewart DJ. A critique of the role of the blood-brain barrier in the chemotherapy of human brain tumors. J Neurooncol 1994;20:121–39. [PubMed: 7807190]
27. van den Bent MJ. The role of chemotherapy in brain metastases. Eur J Cancer 2003;39:2114–20. [PubMed: 14522368]
28. Vick NA, Khandekar JD, Bigner DD. Chemotherapy of brain tumors. Arch Neurol 1977;34:523–6. [PubMed: 889492]
29. Fine R, Chen J, Balmaceda C, Bruce J, Huang M, Desai M, et al. Randomized study of paclitaxel and tamoxifen deposition into human brain tumors: Implications for the treatment of metastatic tumors. Clin Cancer Res 2006;12:5770–6. [PubMed: 17020983]
30. Heimans J, Vermorken J, Wolbers J, Eeltink C, Meijer O, Taphoorn M, et al. Paclitaxel (TAXOL) concentrations in brain tumor tissue. Annals of Oncology 1994;5:951–4. [PubMed: 7696168]
31. Lien E, Wester K, Lonning P, Solheim E, Ueland P. Distribution of tamoxifen and metabolites into brain tissue and brain metastases in breast cancer patients 1991;51:4837–44.
32. Wang F, Zhou F, Kruh GD, Gallo JM. Influence of blood-brain barrier efflux pumps on the distribution of vincristine in brain and brain tumors. Neuro Oncol. 2010
33. Thomas FC, Taskar K, Rudraraju V, Goda S, Thorsheim HR, Gaasch JA, et al. Uptake of ANG1005, a novel paclitaxel derivative, through the blood-brain barrier into brain and experimental brain metastases of breast cancer. Pharm Res 2009;26:2486–94. [PubMed: 19774344]
34. Gallo JM, Li S, Guo P, Reed K, Ma J. The effect of P-glycoprotein on paclitaxel brain and brain tumor distribution in mice. Cancer Res 2003;63:5114–7. [PubMed: 12941842]
35. Fellner S, Bauer B, Miller DS, Schaffrik M, Fankhanel M, Spruss T, et al. Transport of paclitaxel (Taxol) across the blood-brain barrier in vitro and in vivo. J Clin Invest 2002;110:1309–18. [PubMed: 12417570]
36. Apparaju SK, Gudelsky GA, Desai PB. Pharmacokinetics of gemcitabine in tumor and non-tumor extracellular fluid of brain: an in vivo assessment in rats employing intracerebral microdialysis. Cancer Chemother Pharmacol 2008;61:223–9. [PubMed: 17443325]
37. Sigmond J, Honeywell RJ, Postma TJ, Dirven CM, de Lange SM, van der Born K, et al. Gemcitabine uptake in glioblastoma multiforme: potential as a radiosensitizer. Ann Oncol 2009;20:182–7. [PubMed: 18701427]
38. von Holst H, Knochenhauer E, Blomgren H, Collins VP, Ehn L, Lindquist M, et al. Uptake of adriamycin in tumour and surrounding brain tissue in patients with malignant gliomas. Acta Neurochir (Wien) 1990;104:13–6. [PubMed: 2386084]
39. Bos P, Zhang X, Nadal C, Shu W, Gomis R, Nguyen D, et al. Genes that mediate breast cancer metastasis to the brain. Nature 2009;459:1005–10. [PubMed: 19421193]
40. Palmieri D, Bronder JL, Herring JM, Yoneda T, Weil RJ, Stark AM, et al. Her-2 overexpression increases the metastatic outgrowth of breast cancer cells in the brain. Cancer Res 2007;67:4190–8. [PubMed: 17483330]
41. Yoneda T, Williams P, Hiraga T, Niewolna M, Nishimura R. A bone seeking clone exhibits different biological properties from the MDA-MB-231 parental human breast cancer cells and a brain-seeking clone in vivo and in vitro. J Bone and Mineral Res 2001;16:1486–95.
42. Fitzgerald D, Palmieri D, Hua E, Hargrave E, Herring J, Qian Y, et al. Reactive glia are recruited by highly proliferative brain metastases of breast cancer and promote tumor cell colonization. Clin Exp Metast 2008;25:799–810.
43. Song HT, Jordan EK, Lewis BK, Liu W, Ganjei J, Klaunberg B, et al. Rat model of metastatic breast cancer monitored by MRI at 3 tesla and bioluminescence imaging with histological correlation. J Transl Med 2009;7:88. [PubMed: 19840404]
44. Tao K, Fang M, Alroy J, Sahagian G. Imagable 4T1 model for the study of late stage breast cancer. BMC Cancer 2008;8:228. [PubMed: 18691423]
45. Blasberg RG, Fenstermacher JD, Patlak CS. Transport of alpha-aminoisobutyric acid across brain capillary and cellular membranes. J Cereb Blood Flow Metab 1983;3:8–32. [PubMed: 6822623]

46. Asotra K, Ningaraj N, Black KL. Measurement of blood-brain and blood-tumor barrier permeabilities with [14C]-labeled tracers. Methods Mol Med 2003;89:177–90. [PubMed: 12958420]
47. Habazettl H, Athanasopoulos D, Kuebler WM, Wagner HE, Roussos C, Wagner PD, et al. Near-infrared spectroscopy and indocyanine green derived blood flow index for non-invasive measurement of muscle perfusion during exercise. J Appl Physiol 2010;108:962–7. [PubMed: 20110542]
48. Vicini P, Bonadonna RC, Lehtovirta M, Groop LC, Cobelli C. Estimation of blood flow heterogeneity in human skeletal muscle using intravascular tracer data: importance for modeling transcapillary exchange. Ann Biomed Eng 1998;26:764–74. [PubMed: 9779948]
49. Gril B, Palmieri D, Bronder JL, Herring JM, Vega-Valle E, Feigenbaum L, et al. Effect of lapatinib on the outgrowth of metastatic breast cancer cells to the brain. J Natl Cancer Inst 2008;100:1092–103. [PubMed: 18664652]
50. Palmieri D, Lockman PR, Thomas FC, Hua E, Herring J, Hargrave E, et al. Vorinostat inhibits brain metastatic colonization in a model of triple-negative breast cancer and induces DNA double-strand breaks. Clin Cancer Res 2009;15:6148–57. [PubMed: 19789319]
51. Eiseman JL, Eddington ND, Leslie J, MacAuley C, Sentz DL, Zuhowski M, et al. Plasma pharmacokinetics and tissue distribution of paclitaxel in CD2F1 mice. Cancer Chemother Pharmacol 1994;34:465–71. [PubMed: 7923556]
52. Zhou Q, Chowbay B. Determination of doxorubicin and its metabolites in rat serum and bile by LC: application to preclinical pharmacokinetic studies. J Pharm Biomed Anal 2002;30:1063–74. [PubMed: 12408897]
53. Smith QR. A review of blood-brain barrier transport techniques. Methods Mol Med 2003;89:193–208. [PubMed: 12958421]
54. Ohno K, Pettigrew KD, Rapoport SI. Local cerebral blood flow in the conscious rat as measured with 14C-antipyrine, 14C-iodoantipyrine and 3H-nicotine. Stroke 1979;10:62–7. [PubMed: 432901]
55. Ottewell PD, Deux B, Monkkonen H, Cross S, Coleman RE, Clezardin P, et al. Differential effect of doxorubicin and zoledronic acid on intraosseous versus extraosseous breast tumor growth in vivo. Clin Cancer Res 2008;14:4658–66. [PubMed: 18628481]
56. Erba PA, Manfredi C, Lazzeri E, Minichilli F, Pauwels EK, Sbrana A, et al. Time course of Paclitaxel-induced apoptosis in an experimental model of virus-induced breast cancer. J Nucl Med 2010;51:775–81. [PubMed: 20395330]
57. Carbonell WS, Ansorge O, Sibson N, Muschel R. The vascular basement membrane as “soil” in brain metastasis. PLoS One 2009;4:e5857. [PubMed: 19516901]
58. Kusters B, Leenders WP, Wesseling P, Smits D, Verrijp K, Ruiter DJ, et al. Vascular endothelial growth factor-A(165) induces progression of melanoma brain metastases without induction of sprouting angiogenesis. Cancer Res 2002;62:341–5. [PubMed: 11809675]
59. Kim LS, Huang S, Lu W, Lev DC, Price JE. Vascular endothelial growth factor expression promotes the growth of breast cancer brain metastases in nude mice. Clin Exp Metastasis 2004;21:107–18. [PubMed: 15168728]
60. Zuniga RM, Torcuator R, Jain R, Anderson J, Doyle T, Ellika S, et al. Efficacy, safety and patterns of response and recurrence in patients with recurrent high-grade gliomas treated with bevacizumab plus irinotecan. J Neurooncol 2009;91:329–36. [PubMed: 18953493]
61. Uehara H, Miyagawa T, Tjuvajev J, Joshi R, Beattie B, Oku T, et al. Imaging experimental brain tumors with 1-aminocyclopentane carboxylic acid and alpha-aminoisobutyric acid: comparison to fluorodeoxyglucose and diethylenetriaminepentaacetic acid in morphologically defined tumor regions. J Cereb Blood Flow Metab 1997;17:1239–53. [PubMed: 9390656]
62. Miyagawa T, Oku T, Sasajima T, Dasai R, Beattie B, Finn R, et al. Assessment of treatment response by autoradiography with (14)C-aminocyclopentane carboxylic acid, (67)Ga-DTPA, and (18)F-FDG in a herpes simplex virus thymidine kinase/ganciclovir brain tumor model. J Nucl Med 2003;44:1845–54. [PubMed: 14602869]

63. Schmidt KC, Smith CB. Resolution, sensitivity and precision with autoradiography and small animal positron emission tomography: implications for functional brain imaging in animal research. Nucl Med Biol 2005;32:719–25. [PubMed: 16243647]
64. Blasberg RG, Shapiro WR, Molnar P, Patlak CS, Fenstermacher JD. Local blood-to-tissue transport in Walker 256 metastatic brain tumors. J Neurooncol 1984;2:205–18. [PubMed: 6502195]
65. Zhang RD, Price JE, Fujimaki T, Bucana CD, Fidler IJ. Differential permeability of the blood-brain barrier in experimental brain metastases produced by human neoplasms implanted into nude mice. Am J Pathol 1992;141:1115–24. [PubMed: 1443046]
66. Jain RK, di Tomaso E, Duda DG, Loeffler JS, Sorensen AG, Batchelor TT. Angiogenesis in brain tumours. Nat Rev Neurosci 2007;8:610–22. [PubMed: 17643088]
67. Kienast Y, von Baumgarten L, Fuhrmann M, Klinkert WE, Goldbrunner R, Herms J, et al. Real-time imaging reveals the single steps of brain metastasis formation. Nat Med 2010;16:116–22. [PubMed: 20023634]
68. Lu W, Bucana C, Schroit A. Pathogenesis and vascular integrity of breast cancer brain metastasis. Int J Cancer 2007;120:1023–6. [PubMed: 17187362]
69. Hasegawa H, Ushio Y, Hayakawa T, Yamada K, Mogami H. Changes of the blood-brain barrier in experimental metastatic brain tumors. J Neurosurg 1983;59:304–10. [PubMed: 6864299]
70. Fenstermacher J, Gross P, Sposito N, Acuff V, Pettersen S, Gruber K. Structural and functional variations in capillary systems within the brain. Ann N Y Acad Sci 1988;529:21–30. [PubMed: 3395069]
71. Kalvass JC, Maurer TS, Pollack GM. Use of plasma and brain unbound fractions to assess the extent of brain distribution of 34 drugs: comparison of unbound concentration ratios to in vivo p-glycoprotein efflux ratios. Drug Metab Dispos 2007;35:660–6. [PubMed: 17237155]
72. Yen WC, Lamph WW. The selective retinoid X receptor agonist bexarotene (LGD1069, Targretin) prevents and overcomes multidrug resistance in advanced breast carcinoma. Mol Cancer Ther 2005;4:824–34. [PubMed: 15897247]
73. Pichot CS, Hartig SM, Xia L, Arvanitis C, Monisvais D, Lee FY, et al. Dasatinib synergizes with doxorubicin to block growth, migration, and invasion of breast cancer cells. Br J Cancer 2009;101:38–47. [PubMed: 19513066]
74. Cardoso F, Brites D, Brito M. Looking at the blood-brain barrier: Molecular anatomy and possible investigational approaches. Brain Res Rev. In press.
75. Al Ahmad A, Gassmann M, Ogunshola OO. Maintaining blood-brain barrier integrity: pericytes perform better than astrocytes during prolonged oxygen deprivation. J Cell Physiol 2009;218:612–22. [PubMed: 19016245]
76. Nishioku T, Dohgu S, Takata F, Eto T, Ishikawa N, Kodama K, et al. Detachment of brain pericytes from the basal lamina is involved in disruption of the blood-brain barrier caused by lipopolysaccharide-induced sepsis in mice. Cell Mol Neurobiol 2009;29:309–16. [PubMed: 18987969]
77. Parkinson FE, Hacking C. Pericyte abundance affects sucrose permeability in cultures of rat brain microvascular endothelial cells. Brain Res 2005;1049:8–14. [PubMed: 15935996]
78. Zozulya A, Weidenfeller C, Galla HJ. Pericyte-endothelial cell interaction increases MMP-9 secretion at the blood-brain barrier in vitro. Brain Res 2008;1189:1–11. [PubMed: 18061148]

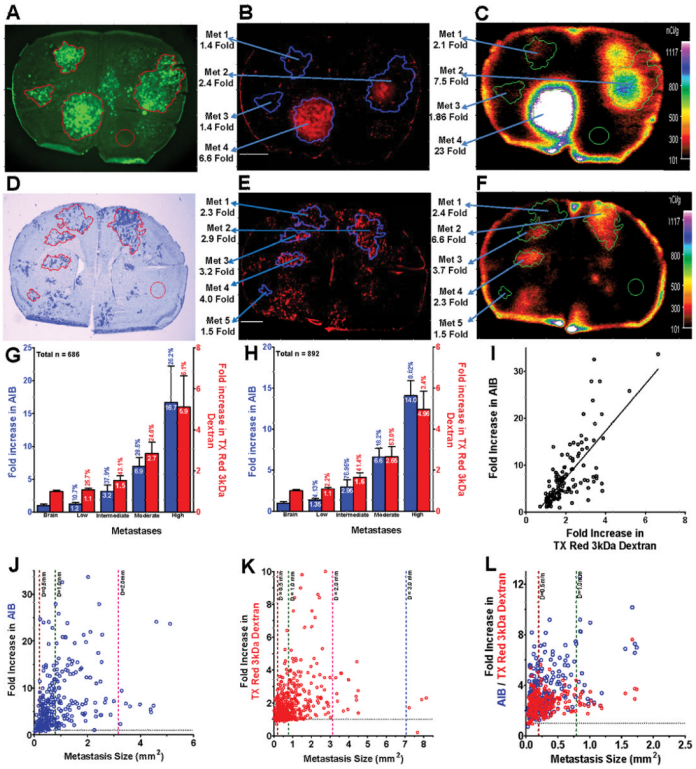

Figure 1. Experimental brain metastases of breast cancer exhibit heterogeneous passive permeability with weak correlation to lesion size

(**A** and **D)** Representative images of metastases of **A:** eGFP-transfected 231-BR-Her2 or **D:** 4T1-BR5 cells (cresyl violet staining), respectively. **B-C and E-F**: Images of the same brain section showing metastases and brain accumulation of Texas Red 3kDa dextran and ^{14}C-AIB with vascular washout. White scale bar represents 1 mm. The fold increase (mean ± SD) in ^{14}C-AIB (blue bars) and TX Red 3kDa dextran (red bars) PS is shown between brain and 231-BR-Her2 brain metastases **(G)** and 4T1-BR5 brain metastases **(H)**. Metastases were separated into four groups based upon the magnitude of the permeability change compared to mean brain. Values represent the percent of metastases in each group, and the mean fold increase of tracer in each group. **I:** Fold increase ^{14}C-AIB (over normal brain) plotted versus fold increase Texas Red 3kDa dextran in 231-BR-Her2 metastases. r^2=0.54, P<0.0001 (n=127). **J and K:** Fold elevation of ^{14}C-AIB (blue dots; n=288) and Texas Red 3kDa dextran (red dots; n=535) in individual 231-BR-Her2 brain metastases compared to brain distant from tumor graphed versus metastasis size (mm^2). Brain distant from tumor equals 1.0 and is represented by the horizontal line. Diameter in one plane is shown in vertical lines. **L:** Fold elevation of metastasis ^{14}C-AIB (blue dots) and Texas Red 3kDa dextran (red dots) versus metastasis size in 4T1-BR5 (n=229).

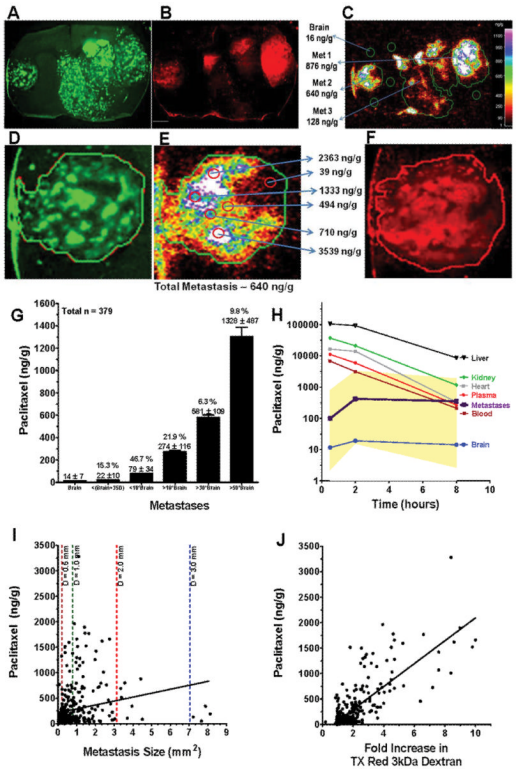

Figure 2. Variable paclitaxel uptake in 231-BR-Her2 brain metastases that correlates with Texas Red 3kDa dextran accumulation

^{14}C-Paclitaxel distribution in 231-BR-Her2 metastases after intravenous administration of 10 mg/kg paclitaxel (Taxol formulation). Distribution of **A:** EGFP, **B:** Texas Red 3kDa dextran (10 min circulation), and **C:** ^{14}C-paclitaxel (8 hr); followed by a 30 s vascular washout. White scale bar represents 1 mm. Heterogeneous distribution is shown within one representative brain metastasis (**D:** EGFP; **E:** ^{14}C-paclitaxel; **F:** Texas Red 3kDa dextran). **G:** ^{14}C-Paclitaxel concentration (ng/g) in brain and 231-BR-Her2 brain metastases. Values represent the percent of all metastases in each group, and the mean ± SD ^{14}C-paclitaxel concentration in each group. **H:** Mean brain metastasis drug concentration was measured at different times (30 min-8 hrs) and related to that in brain distant from tumor, plasma, blood, and peripheral tissues (n=3 animals per point). Yellow areas show highest and lowest concentrations observed in brain metastases at the three time points. Calculated area under the curve cumulative exposure (in μg.hr/g) equaled 0.18 in brain, 2.9 in average brain metastasis, and 80-400 in peripheral tissues. **I:** The ^{14}C-paclitaxel concentration versus lesion size of individual metastasis are graphed for 231-BR-Her2. Correlation was minimal between brain metastasis paclitaxel concentration and lesion size (Pearson r^2=0.037). Dashed lines represent diameter. **J:** Correlation of ^{14}C-paclitaxel concentration versus fold increase of Texas Red 3kDa dextran permeability of individual metastases. An appreciable correlation of paclitaxel concentration to Texas Red 3kDa dextran was noted (Pearson r^2=0.605, P<0.0001, n=354).

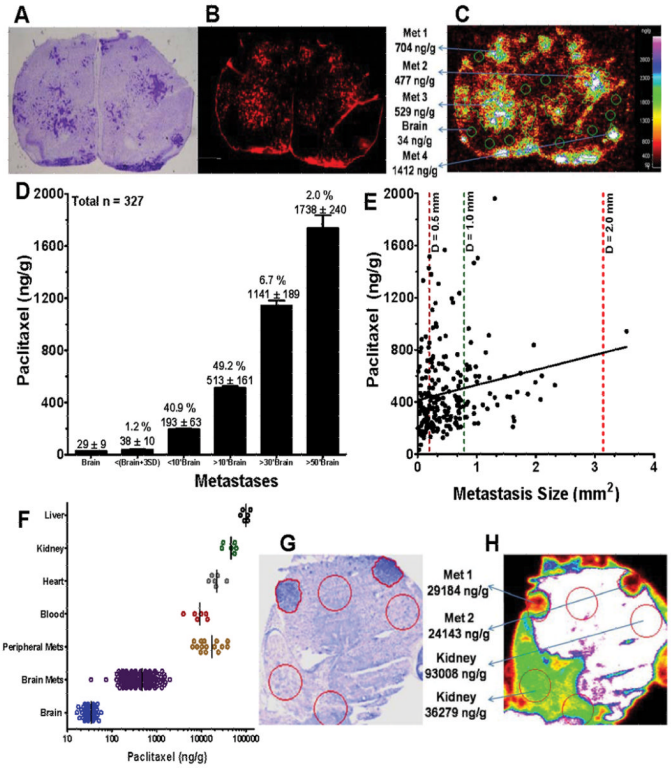

Figure 3. Variable paclitaxel uptake in 4T1-BR5 brain metastases of breast cancer

A-C: ^{14}C-Paclitaxel distribution in representative 4T1-BR5 brain metastases. TX Red 3kDa permeability marker circulated for 10 min whereas 10 mg/kg ^{14}C-paclitaxel circulated for 30 min (after circulation of both tracers there was a 30 s vascular washout) **A:** Bright field image of cresyl violet stained lesions. **B:** Texas Red 3kDa dextran uptake (White scale bar represents 1 mm). **C:** ^{14}C-Paclitaxel concentration. **D:** ^{14}C-Paclitaxel concentration (ng/g) in brain and 4T1-BR5 brain metastases. **E:** ^{14}C-Paclitaxel concentration versus lesion size of individual metastases. Correlation was minimal between brain metastasis paclitaxel concentration and lesion size (Pearson r^2=0.034). Dashed lines represent diameter. **F:** ^{14}C-paclitaxel distribution (30 min) in 4T1-BR5 metastases in brain and peripheral tissues, as well as in matching surrounding normal tissues. The distribution of individual data points for brain and peripheral tissues are shown as well as the mean. N=3 mice. **G:** Representative section showing cresyl violet stained 4T1-BR5 kidney metastases: **H:** ^{14}C-paclitaxel concentration in kidney section.

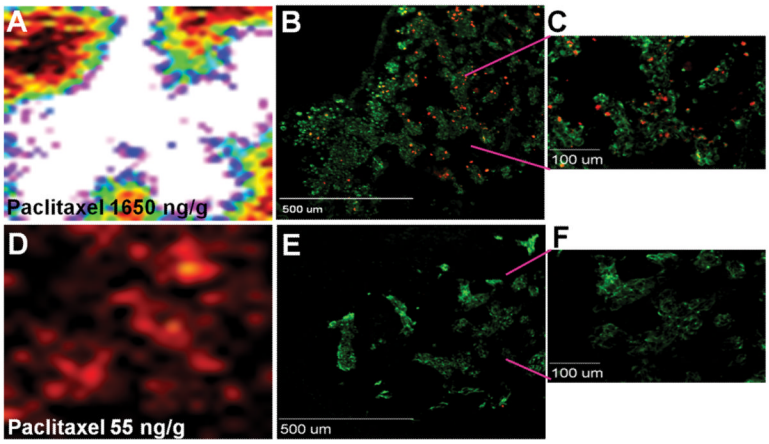

Figure 4. Positive cleaved caspase-3 staining in brain metastases with high paclitaxel accumulation

Representative images of **A:** high (representing <10% of lesions) and **D:** low ^{14}C-paclitaxel uptake in 231-BR-Her2 experimental metastases. Presence of cleaved caspase-3 staining (red) was found in human cytokeratin positive tumor cells (green) within brain metastases with markedly elevated paclitaxel concentration (**B-C**), but not in metastases with low paclitaxel concentration (**E-F**). N=3-5 animals per group.

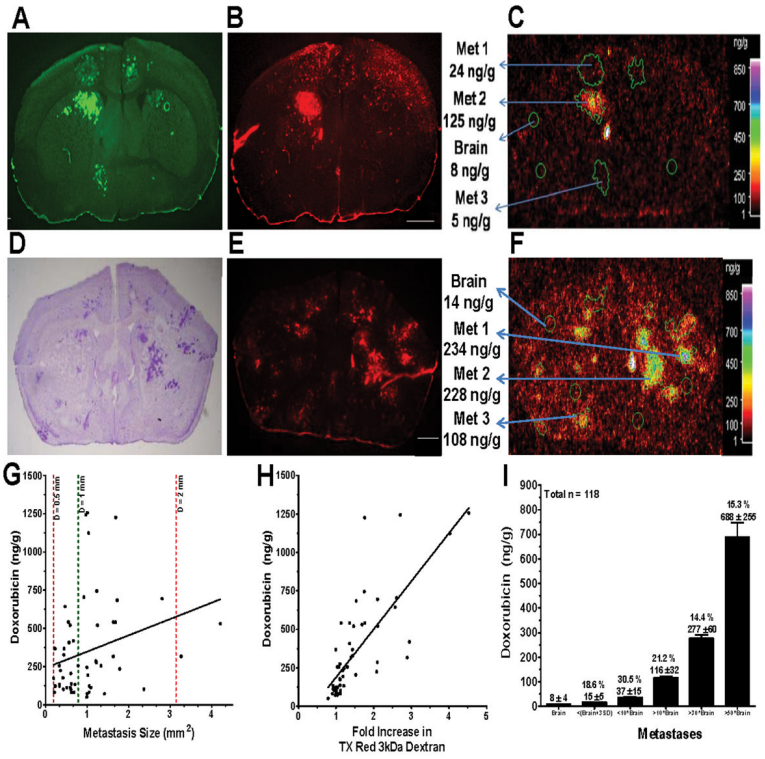

Figure 5. Heterogeneous doxorubicin uptake in 231-BR-Her2 brain metastases of breast cancer

^{14}C-Doxorubicin distribution in representative images for 231-BR-Her2 (**A-C**) and 4T1BR5 **(D-F)** brain metastases. TX Red 3kDa permeability marker circulated for 10 min whereas 6 mg/kg ^{14}C-doxorubicin circulated for 30 min; followed by a 30 s vascular washout. **A:** EGFP imaging. **D**: Cresyl violet staining, **B** and **E:** Texas Red 3kDa dextran uptake. **C** and **F:** ^{14}C-Doxorubicin uptake. **G:** ^{14}C-Doxorubicin concentration versus lesion size of individual metastases. Correlation was minimal between brain metastasis doxorubicin concentration and lesion size (Pearson r^2=0.070). Dashed lines represent diameter. **H:** ^{14}C-Doxorubicin correlated appreciably with fold increase in Texas Red 3kDa dextran permeability (Pearson r^2=0.591, P<0.0001, n=54). Serum ^{14}C was shown to be >95% intact ^{14}C-doxorubicin at 30 min of circulation using HPLC. **I:** ^{14}C-Doxorubicin concentration (ng/g) in brain and 231-BR-Her2 brain metastases. Metastases were separated into five groups based upon the magnitude of the ^{14}C-doxorubicin concentration relative to normal brain. Values represent the percent of all metastases in each group, and the mean ± SD ^{14}C-doxorubicin concentration in each group.

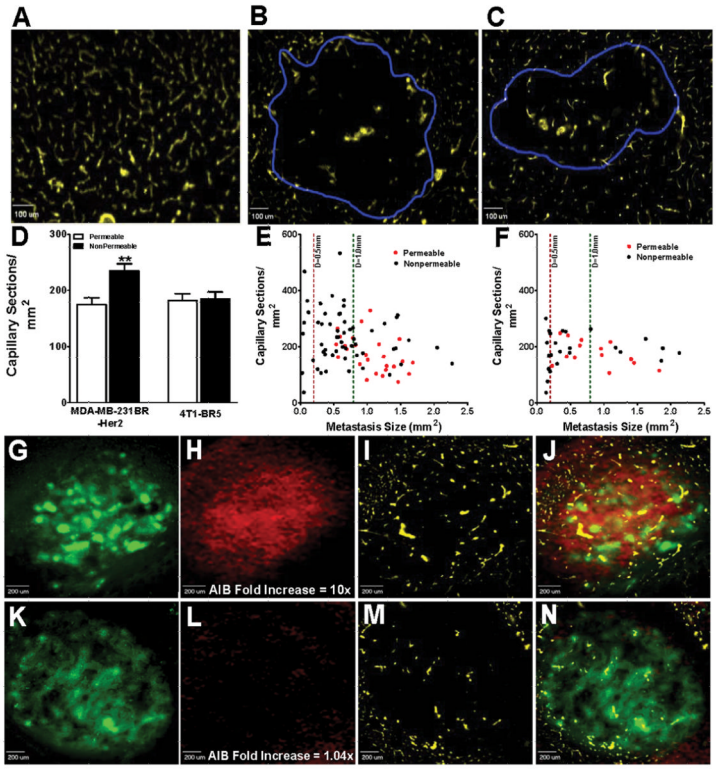

Figure 6. Vascular density is reduced and does not correlate with BTB permeability in two experimental models of brain metastasis of breast cancer

Representative images of the vascular density of **A:** normal brain, **B:** 231-BR-Her2, and **C:** 4T1-BR5 metastases (capillaries, yellow; metastasis boundary, blue). **D:** Calculated vascular densities of both permeable and non-permeable metastases. **E** and **F:** Vascular density and metastasis size for permeable and nonpermeable tumors. **E:** 231-BR-Her2. **F:** 4T1-BR5. Data were obtained by injection and circulation of ^{14}C-AIB (10 min) and indocyanine green (1 min) bound to albumin as the vascular tracer. Elevated BTB permeability was not associated with increased vascular density either by analysis of linear regression slopes or intercepts ($P>0.05$). Representative images showing simultaneous multi-channel quantitative imaging of eGFP (**G and K**), ^{14}C-AIB by phosphorescent imaging (**H and L**), vascular density by near infrared imaging of indocyanine green (**I and M**) of a permeable (**G-J**) and non-permeable lesion (**K-N**); **J and N** are combined multichannel images.

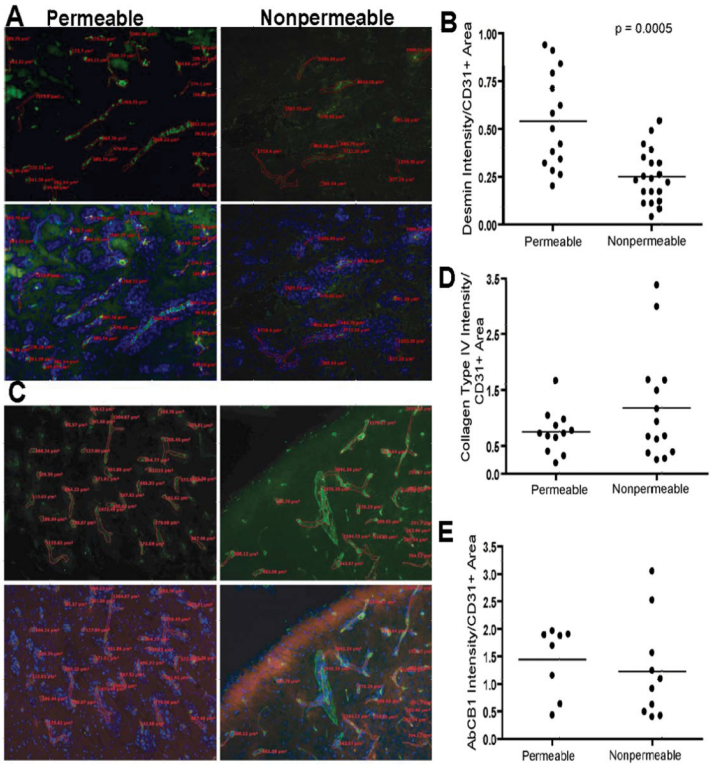

Figure 7. Passive permeability of experimental brain metastases is associated with blood-tumor barrier remodeling

A: BTB permeability is associated with desmin overexpression by immunoflourescent staining. Representative images of desmin staining in adjacent permeable and nonpermeable metastases from the same brain. CD31 (capillaries, red), desmin (green) and DAPI (nuclei, blue). **B:** Desmin expression per CD31+ area plotted for 35 permeable and nonpermeable metastases. Mean values are indicated as lines. Expression intensity was ~2 fold elevated in permeable versus nonpermeable metastases (P=0.0005, Mann-Whitney test). **C:** Representative section stained for type IV collagen (green). Other colors same as **A**. **D-E:** Plotted data for type IV collagen and ABCB1 (P>0.05).